pISSN 1229-3008 eISSN 2287-6251
Progress in Superconductivity and Cryogenics
Vol.23, No.4, (2021), pp.1~5 https://doi.org/10.9714/psac.2021.23.4.001

Dependence of superconductivity on the crystallinity of Nb films on Si wafers

Joonyoung Choi, Chang-Duk Kim[+], and Younjung Jo[*]

Kyungpook National University, Daegu, Korea

(Received 18 December 2021; revised or reviewed 29 December 2021; accepted 30 December 2021)

Abstract

Among elemental metals, niobium (Nb) has the highest superconducting transition temperature (T_c) at ambient pressure. Thus, Nb films have been used in superconducting electronics and radio frequency cavity applications. In this study, the depositional factors determining the crystallinity and T_c of Nb films were investigated. An Nb film grown at a sputtering temperature of 240℃ exhibited the maximum crystallinity of Nb and the minimum crystallinity of niobium oxide. X-ray photoelectron spectroscopy confirmed a maximum atomic percent of niobium and a minimum atomic percent of oxygen. A sputtering power of 210 W and a sputtering time of 50 min were the optimal conditions for Nb deposition, and the T_c of the optimized film (9.08 K) was close to that of bulk Nb (9.25 K). Transmission electron microscopy images of the thick film directly confirmed the removal of the typical in-plane compressive strain in the (110) plane caused by residual stress.

Keywords: critical fields; critical temperature; films, niobium compounds; sputtering; superconducting material growth

1. INTRODUCTION

Niobium (Nb) is a type II superconductor with a body-centered cubic (bcc) structure. It has a bulk critical temperature (T_c) of approximately 9.25 K and a very large magnetic penetration depth [1, 2]. Among elements, Nb has the highest T_c; thus, it is utilized in various types of laboratory physics equipment, for example, in superconducting radio frequency cavities in X-ray free-electron lasers and the International Linear Collider facility [3, 4], as well as in diffusion-cooled hot-electron bolometers [5]. However, the use of bulk Nb in such experimental equipment is costly. Conversely, when an Nb thin film is used, the upper critical field can be increased while reducing the cost [2, 3]. Therefore, the fabrication of Nb thin films that exhibit bulk-level superconducting properties has gained considerable attention. To fabricate Nb thin films with high T_c, various studies have utilized substrates of quartz [5], sapphire [6], magnesium oxide [7], porous silicon [8], borosilicate [9], copper (Cu) [7], or aluminum oxide [10]. When the lattice constant and thermal expansion coefficient of the substrate material are similar to those of Nb, an Nb thin film with a T_c as high as that of bulk Nb can be deposited [11]. However, owing to problems in the film application process as well as cost constraints, Nb thin films are commonly required to be applied to a Si substrate, which is of low cost and wide usage. We have already reported how the internal strain caused by the lattice constant mismatch between Nb and Si affects T_c. In particular, in-plane compressive strain in the (110) plane due to residual stress reduces the T_c [12, 13]. In the present study, Nb films attaining bulk-level T_c were deposited on a Si substrate via DC magnetron sputtering. Optimal deposition conditions were determined by controlling factors such as substrate temperature during deposition, sputtering power, and sputtering time. The structural and surface characteristics of the fabricated Nb thin films were also investigated. A key sputtering condition-related correlation between crystallinity and T_c was identified.

* Corresponding author: jophy@knu.ac.kr
+ Corresponding author: duks@knu.ac.kr

2. EXPERIMENTAL

Nb films were grown on Si substrates via DC magnetron sputtering [12, 13]. A P-type Si ⟨100⟩ wafers having a thickness of 530 μm and retaining its native oxide layer was cut into 10 × 10 mm^2 squares and rinsed. The base vacuum level was fixed at 1.0×10^{-5} Torr, and the film was grown at an argon pressure of 1.6 mTorr with an Ar gas flow rate of 20 sccm. Selected independent variables describing Nb film deposition conditions were Si substrate temperature (T_s = 27℃, 150℃, 200℃, 240℃, 250℃, and 300℃), sputtering power (120, 150, 180, 210, 240, and 270 W), and sputtering time (10, 20, 30, 40, and 50 min). Films of 240℃, 150 W, and 30 minutes for each variable were re-made and analyzed in consideration of the change in putting condition. Surface and structural characteristics were measured using a field-emission scanning electron microscope (FESEM, Hitachi SU8220). An X-ray diffractometer (XRD, PANalytical MPD) using Cu Kα radiation (wavelength, 1.541 Å) at a current of 30 mA and voltage of 40 kV was also employed. A $2\theta/\omega$ scan was performed in the range of 20°–80° with 0.01° steps. X-ray

photoelectron spectroscopy (XPS, Thermo Fisher KA1149) and transmission electron microscopy (TEM, FEI Tecnai G2 F20) were also utilized. Temperature-dependent resistance $R(T)$ was measured using a four-point probe method while reducing the temperature from 300 to 4 K. Temperature was reduced at a rate of 2 K/min down to the base temperature. T_c was then measured by heating each Nb film at a rate of 0.1 K/min. The T_c value was derived from the maximum value of the first derivative of $R(T)$.

3. RESULTS AND DISCUSSION

Figure 1 shows the structural and electrical properties of Nb films deposited at various temperatures: room temperature, 150℃, 200℃, 240℃, 250℃, and 300℃. The temperature of the Si substrate (T_s) on which each Nb film was deposited was kept constant by installing a halogen lamp and a temperature controller on the back side of the Si substrate. The sputtering power and sputtering time were fixed at 150 W and 30 min, respectively. Figure 1(a) presents scanning electron microscopy (SEM) images of the surfaces of the Nb films, with each surface state forming differently depending on T_s. At temperatures of 150℃ and 200℃, since the Nb film had a large protrusion formed between small protrusions on the surface, it was expected that two or more crystalline states would be formed. Nb films deposited at T_s below 200℃ were amorphous, consistent with findings from previous reports [14]. According to Thornton and extended structure zone diagrams, the columnar structure and topography of the sputtered film were profoundly affected by T_s [12, 15–17]. Although all T_s values were less than or equal to one-tenth of the melting temperature of Nb (~2477℃), the morphological change seems to extend through Zone 1, Zone T (transition), and Zone 2 in the diagram.

XRD measurements, as shown in Figure 1(b) and (c), can also be expected to reveal different crystal structures of the Nb film depending on T_s [12, 18]. The XRD peaks of Nb films included peaks for Nb (JCPDS 02-1108), Nb_2O_5 (JCPDS 30-0872), and NbO (JCPDS 15-0535). At room temperature, only peaks corresponding to oxides were formed [19]. Remarkably, Nb (110) and Nb (211) peaks representing Nb were formed at 200℃, with the highest of such peak observed at 240℃. At 250℃, the intensity of the Nb (110) and Nb (211) peaks slightly decreased, the Nb_2O_5 peak was relatively high, and the Nb (200) peak was newly formed. At 300℃, the Nb_2O_5 and NbO peaks, which had not been identified at lower temperatures, appeared near the Nb (110) and Nb (211) peaks, and the Nb_2O_5 peak was very high. It has been reported that Nb films prefer to form the most favorable state of Nb_2O_5 at equilibrium conditions given sufficient oxygen [20]. The minute amount of oxygen remaining in the chamber or oxygen from the substrate [21] can also react during the formation of the Nb film given a high deposition temperature [7, 12, 22, 23]. It is known that NbO crystals are formed by reduction during the heat treatment process of Nb_2O_5 crystals [24]. As an aid in identifying the crystallinity of the Nb film, Figure 1(c)

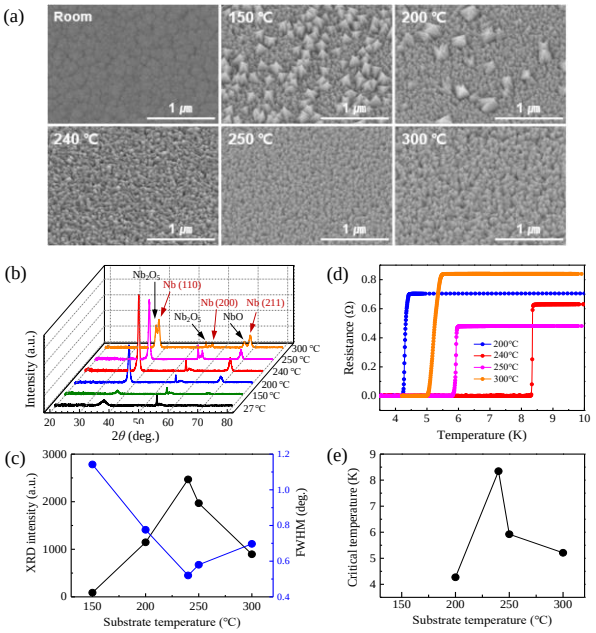

Fig. 1. Structural and electrical characteristics of Nb films deposited at various deposition temperatures. (a) Scanning electron microscopy images of Nb films, (b) X-ray diffractometer (XRD) measurements performed on deposited Nb films, (c) integrated XRD intensity and full width at half maximum (FWHM) of the Nb (110) peak, (d) superconducting transitions of Nb films, and (e) critical temperatures (T_c) of Nb films with respect to the Si substrate temperature [12].

shows the XRD intensity and full width at half maximum (FWHM) for the Nb (110) peak, which was the main peak. At 240℃, the XRD intensity of the Nb (110) peak was at its highest, whereas the FWHM was at its lowest. Thus, the crystallinity of Nb (110) was at its highest at 240℃. The superconducting transition characteristics of the Nb films were determined by measuring the temperature-dependent resistance $R(T)$ (Figure 1(d)). The Nb film deposited at room temperature exhibited insulating behavior, and superconducting transition was not observed in the Nb films deposited below 200℃. For films deposited at or above 200℃, a sharp superconducting transition of zero resistance occurred at low temperature. T_c was defined by the maximum differential value of resistance, i.e., dR/dT. T_c reached its maximum of 8.34 K in the Nb film deposited at 240℃, whereas the T_c values for Nb films deposited at 200℃, 240℃, 250℃, and 300℃ were found to be 4.29, 8.34, 5.92, and 5.21 K, respectively. Figure 1(e) indicates that the tendency of T_c is similar to that of the Nb (110) peak intensity in XRD (Figure 1(c)).

We further note that niobium oxide is formed by the reaction of Nb crystals and O_2 during deposition. To identify the relationship between the T_c, chemical composition, and chemical state of Nb films, XPS measurements were performed. After surface milling of approximately 50 nm using Ar^+ ions, XPS analysis was conducted. Figure 2(a) presents the XPS peaks at various T_s values. Here, each peak for Nb and niobium oxide can be distinguished by a different color [25–27]. At the T_s value

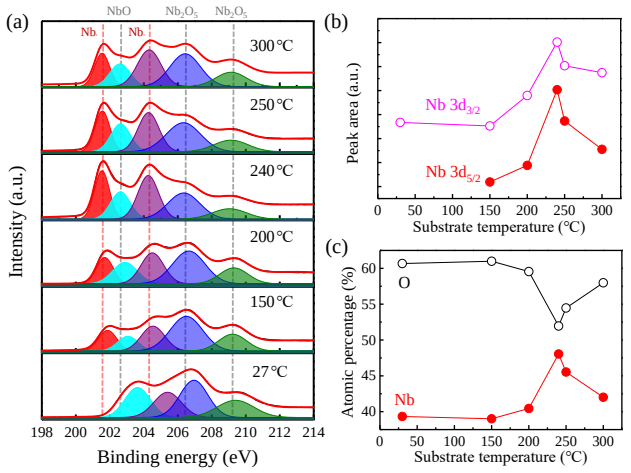

Fig. 2. (a) X-ray photoelectron spectroscopy analysis of Nb and NbO peaks, (b) peak area for Nb $3d_{3/2}$ and $3d_{5/2}$, and (c) atomic percentages of Nb and O as functions of substrate temperature.

of 27℃, four peaks were identified at binding energies of 203.7, 205.4, 207.0, and 209.4 eV via peak separation. At T_s values of 150℃ or higher, a new peak in the 201.6 eV region was formed, resulting in a total of five peaks. As T_s increased, the peaks shifted to lower binding energies, but above 240℃, the peak positions became fixed. The peaks were fixed at binding energies of 201.6, 202.6, 204.3, 206.4, and 209.1 eV. The chemical states of the Nb atoms can be accurately interpreted from the positions of the corresponding lines in the photoelectron energy spectrum [26]. Typically in bulk Nb materials, the core-level spectra of Nb $3d_{5/2}$ and Nb $3d_{3/2}$ lie at 202.5 and 205.2 eV, respectively [28–30]. The Nb_2O_5 peaks lie at 205, 208, and 210 eV, and the NbO peaks lie at 203 and 206 eV [25–27]. Comparison with our XPS results suggests that all of our XPS peaks appeared at binding energies approximately 1 eV lower than that in typical bulk Nb materials. Considering that the typical peak position of O 1s is around 530.6 eV [31], the binding energy of O 1s here was determined to be 529.7 eV. Therefore, the identities of the binding energies of 201.6, 202.6, 204.3, 206.4, and 209.1 eV were determined to be Nb (Nb $3d_{5/2}$), NbO (Nb $3d_{5/2}$), Nb (Nb $3d_{3/2}$), Nb_2O_5 (Nb $3d_{5/2}$), and Nb_2O_5 (Nb $3d_{3/2}$), respectively. A doublet of Nb $3d_{5/2}$ and Nb $3d_{3/2}$ bands corresponds to each of the mentioned states of the Nb film in the photoelectron spectrum at certain binding energies. In Figure 2(b), the peak areas of Nb $3d_{3/2}$ and $3d_{5/2}$ are presented as functions of T_s. The Nb peaks reach their highest at 240℃, whereas those of Nb_2O_5 reach their lowest at 240℃ (not shown). In Figure 2(c), the atomic percentages of Nb and O are presented. The atomic percentage of Nb increased as the deposition temperature of the Nb film increased and then decreased beyond a T_s of 240℃, but the atomic percentage of oxygen exhibited an opposite trend. These findings suggest that the superconducting properties of the Nb films were significantly affected by the crystallinity of the Nb and oxide components [32, 33].

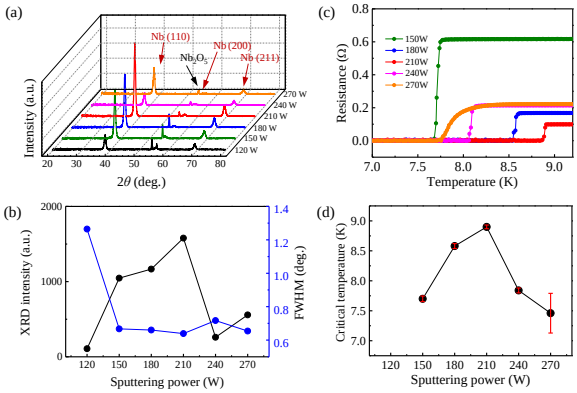

Fig. 3. Structural and electrical characteristics of Nb films deposited at various sputtering power: (a) X-ray diffractometer (XRD) measurements performed on deposited Nb films, (b) integrated XRD intensity and full width at half maximum (FWHM) of the Nb (110) peak, (c) superconducting transitions of Nb films, and (d) T_c values of Nb films with respect to sputtering power. The broadening of the superconducting transition is indicated by error bars.

Figure 3(a) and (b) present the XRD characteristics of the Nb film as functions of sputtering power. The sputtering temperature was fixed at 240℃ to maximize T_c, and the sputtering time was fixed at 30 min. The Nb (110) peak intensity and FWHM shown in Figure 3(b) demonstrate that the crystallinity of Nb increased with increasing sputtering power and then decreased beyond a power of 210 W. Similar to the Nb (110) peak, the crystallinity tendency of Nb with sputtering power was consistent with the peaks for Nb_2O_5, Nb (200), and Nb (211). Figure 3(c) shows $R(T)$ for the Nb films at various sputtering powers. At a sputtering power of 210 W, T_c was found to reach its maximum value of 8.9 K, indicating that the tendency of T_c followed that of the XRD Nb (110) peak intensity (Figure 3(b)).

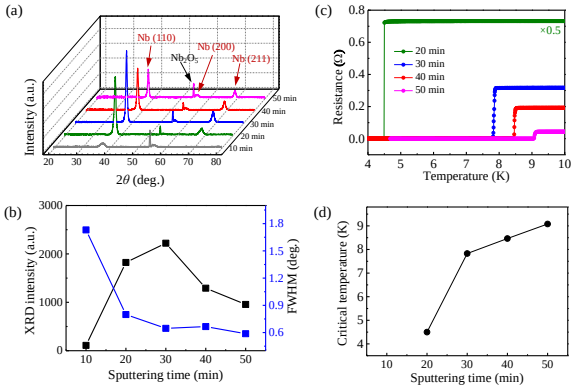

Fig. 4. Structural and electrical characteristics of Nb films deposited for various sputtering times: (a) X-ray diffractometer (XRD) measurements performed on deposited Nb films, (b) integrated XRD intensity and full width at half maximum (FWHM) of the Nb (110) peak, (c) superconducting transitions of Nb films, and (d) T_c values of Nb films with respect to sputtering time.

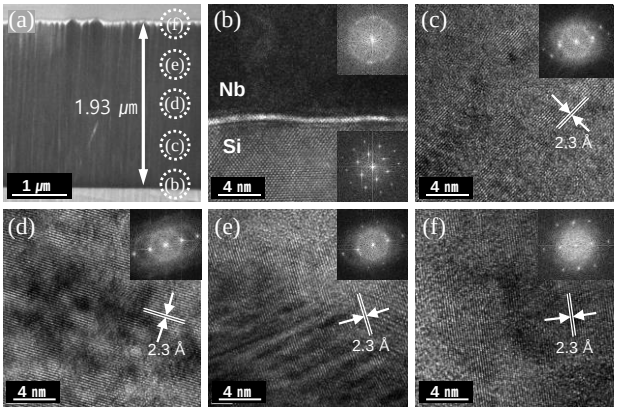

Fig. 5. Transmission electron microscopy (TEM) images of an Nb film deposited for 50 min under sputtering conditions of 240℃ and 210 W. (a) Overall profile of the Nb film and location of the thickness measurement obtained from the image. (b) Interface between the silicon substrate and Nb film. (c–f) The sputtering time and corresponding thickness of the film at each location indicated in (a) are (c) 20 min and 0.79 μm, (d) 30 min and 1.23 μm, (e) 40 min and 1.64 μm, and (f) 50 min and 1.93 μm. The inset in each panel shows the corresponding fast Fourier transform image.

Figure 4(a) and (b) present the XRD characteristics of Nb films as a function of sputtering time. Sputtering temperature was fixed at 240℃, and sputtering power was fixed at 210 W, again maximizing T_c. The XRD spectra for all sputtering times consisted of peaks for Nb (JCPDS 02-1108) and Nb_2O_5 (JCPDS 30-0872). However, the XRD characteristics according to the sputtering time tended to differ slightly from those according to T_s or sputtering power. According to T_s or sputtering power, the XRD intensity and FWHM curves exhibited the same tendency for the crystallinity of the Nb (110) peak. In the case of sputtering time, however, the XRD intensity increased up to a sputtering time of 30 min and then decreased, but the FWHM dropped sharply at 20 min and then gradually decreased. The superconducting transition characteristics presented in Figure 4(c) and (d) exhibit the same tendency as the FWHM of the Nb (110) peak. The maximum T_c of 9.08 K was obtained in the Nb film sputtered for 50 min.

In the Nb (110) structure of the Nb film fabricated under sputtering conditions of 240℃ and 210 W, crystallinity and T_c increased with increasing deposition time, as presented in Figure 4. To directly check the crystallinity of the Nb film as a function of sputtering time, TEM analysis was conducted using the Nb film sputtered for 50 min. The Nb film was sampled using a focused ion beam. The thickness of the deposited Nb film increased at a constant rate. Thus, at a sputtering time of 50 min, it exhibited a thickness of 1.93 μm. The TEM images and results of the fast Fourier transform (FFT) for each location indicated in Figure 5(a) are presented in Figure 5(b)–(f), as well as in the inset of each figure. The deposition time and corresponding thickness of the films were as follows: (c) 20 min and 0.79 μm, (d) 30 min and 1.23 μm, (e) 40 min and 1.64 μm, and (f) 50 min and 1.93 μm. In Figure 5(b), the crystallinity near the boundary where the Nb film began accumulating on the Si substrate was amorphous. Normally, the first 10 nm of Nb thickness does not form an epitaxy, and oxygen from the substrate is therefore incorporated into the Nb. The boundary, filled with stabilizing Nb_2O_5, includes an $Nb–NbO_x–Nb_2O_5$ transition layer on top of which columnar Nb grains are subsequently grown [21]. As the sputtering time increases, patches of the Nb crystal structure begin to form, and eventually, a recognizable Nb crystal structure appears over the entire region. In the FFT image, a uniform lattice can be increasingly easily observed as the sputtering time increases. This trend indicates that the lattice spacing, determined to be 2.3 Å, is well aligned in the Nb (110) direction. The shorter the sputtering time is, the greater is the number of Nb (110) lattices that propagate in different directions or are not identified at all. The longer the sputtering time is, the higher is the crystallinity of the Nb film, and thus, the higher is the T_c.

4. CONCLUSIONS

In this study, we investigated the superconducting properties of Nb films according to substrate temperature, sputtering power, and sputtering time. The crystallinity of Nb and NbO was confirmed using XRD, FESEM, and TEM. Temperature-dependent resistance as a function of sputtering conditions was measured to confirm the superconducting transition phenomenon of the Nb film. The maximum crystallinity of Nb and the minimum crystallinity of NbO were confirmed in the Nb film fabricated under deposition conditions of 240℃, 210 W, and 50 min. The maximum T_c was 9.08 K, closely approaching the bulk Nb transition temperature of 9.25 K. These findings confirm that the crystallinity of sputtered Nb is the most significant factor determining the superconducting properties of the Nb film.

ACKNOWLEDGMENT

This work was funded by the National Research Foundation of Korea (NRF), Nos. NRF-2019R1A2C1089017 and NRF-2019R1I1A1A01061738; and the Ministry of SMEs and Startups (MSS, Korea), No. S2912700.

REFERENCES

[1] M. Peiniger and H. Piel, "A superconducting Nb_3Sn coated multicell accelerating cavity," IEEE Transactions on Nuclear Science, vol. NS-32, no. 5, p. 3610, 1985.

[2] D. K. Finnemore, T. F. Stromberg, and C. A. Swenson, "Superconducting Properties of High-Purity Niobium," Physical Review, vol. 149, no. 1, p. 231, 1966, doi: 10.1103/PhysRev.149.231.

[3] L. N. Hand, J. P. Craig, and W. R. Frisken, "Characterization of Niobium films and a bulk Niobium sample with RRR, SIMS and a SQUID Magnetometer," Proceedings of the 11th Workshop on RF

Superconductivity (SRF' 03), Lübeck, Germany, Sep. 2003 paper THP07, p. 604, 2003.
[4] M. Delheusy et al., "X-ray investigation of subsurface interstitial oxygen at Nb/oxide interfaces," Applied Physics Letters, vol. 92, no. 10, p. 101911, 2008, doi: 10.1063/1.2889474.
[5] M. Frommberger et al., "Properties of Nb thin films and their application for diffusion cooled Hot-Electron Bolometer," Proceedings of the 11th International Symposium on Space Terahertz Technology, edited by A. Ann(University of Michigan, MI USA, 2000), p. 489, 2000.
[6] C. Delacour et al., "Persistence of superconductivity in niobium ultrathin films grown on R-plane sapphire," Physical Review B, vol. 83, no. 14, p. 144504, 2011, doi: 10.1103/PhysRevB.83.144504.
[7] W. M. Roach et al., "Niobium thin film deposition studies on copper surfaces for superconducting radio frequency cavity applications," Physical Review Special Topics - Accelerators and Beams, vol. 15, no. 6, p. 062002, 2012, doi: 10.1103/PhysRevSTAB.15.062002.
[8] M. Trezza et al., "Superconducting properties of Nb thin films deposited on porous silicon templates," Journal of Applied Physics, vol. 104, no. 8, p. 083917, 2008, doi: 10.1063/1.3006014.
[9] E. Valderrama et al., "Nb film growth on crystalline and amorphous subsrates," Proceedings of 15th International Conference on RF Superconductivity, Chichgo, USA, p. 898, 2011.
[10] N. N. Iosad, T. M. Klapwijk, S. N. Polyakov, V. V. Roddatis, E. K. Kov'ev, and P. N. Dmitriev, "Properties of DC magnetron sputtered Nb and NbN films for different source conditions," IEEE Transactions on Applied Superconductivity, vol. 9, no. 2, p. 1720, 1999.
[11] G. i. Oya, M. Koishi, and Y. Sawada, "High-quality single-crystal Nb films and influences of substrates on the epitaxial growth," Journal of Applied Physics, vol. 60, no. 4, p. 1440, 1986, doi: 10.1063/1.337323.
[12] J. Choi et al., "Analysis of the Superconducting Characteristics of Niobium Thin Films Deposited by Using a DC Magnetron Sputtering System," New Physics: Sae Mulli, vol. 68, no. 3, p. 284, 2018, doi: 10.3938/npsm.68.284.
[13] J. Choi, Y.-K. Kim, C.-D. Kim, S. Kim, and Y. Jo, "Enhancing the critical temperature of strained Niobium films," Materials Research Express, vol. 7, no. 7, p. 076001, 2020, doi: 10.1088/2053-1591/aba84a.
[14] L. R. Nivedita, A. Haubert, A. K. Battu, and C. V. Ramana, "Correlation between Crystal Structure, Surface/Interface Microstructure, and Electrical Properties of Nanocrystalline Niobium Thin Films," Nanomaterials, vol. 10, no. 7, Jun 30 2020, doi: 10.3390/nano10071287.
[15] J. A. Thornton, "Influence of apparatus geometry and deposition conditions on the structure and topography of thick sputtered coatings," Journal of Vacuum Science and Technology, vol. 11, no. 4, pp. 666-670, 1974, doi: 10.1116/1.1312732.
[16] A. Anders, "A structure zone diagram including plasma-based deposition and ion etching," Thin Solid Films, vol. 518, no. 15, pp. 4087-4090, 2010, doi: 10.1016/j.tsf.2009.10.145.
[17] M. Maniruzzaman and A. Noya, "Interpretation of Cu(111)//Nb(110) growth on SiO_2 by transmission electron microscopy," 5th International Conference on Electrical and Computer Engineering ICECE 2008, 20-22 December 2008, Dhaka, Bangladesh, p. 812, 2008.
[18] E. Pehlivan and G. A. Niklasson, "Fractal dimensions of niobium oxide films probed by protons and lithium ions," Journal of Applied Physics, vol. 100, no. 5, p. 053506, 2006, doi: 10.1063/1.2337164.
[19] S. J. Rezvani et al., "Substrate-Induced Proximity Effect in Superconducting Niobium Nanofilms," Condensed Matter, vol. 4, no. 1, 2019, doi: 10.3390/condmat4010004.
[20] S. Venkataraj, R. Drese, C. Liesch, O. Kappertz, R. Jayavel, and M. Wuttig, "Temperature stability of sputtered niobium–oxide films," Journal of Applied Physics, vol. 91, no. 8, pp. 4863-4871, 2002, doi: 10.1063/1.1458052.
[21] J. Halbritter, "Transport in superconducting niobium films for radio frequency applications," Journal of Applied Physics, vol. 97, no. 8, 2005, doi: 10.1063/1.1874292.
[22] O. V. Dobrovolskiy and M. Huth, "Crossover from dirty to clean superconducting limit in dc magnetron-sputtered thin Nb films," Thin Solid Films, vol. 520, no. 18, p. 5985, 2012, doi: 10.1016/j.tsf.2012.04.083.
[23] T. J. Hwang and D. H. Kim, "Transition temperatures and upper critical fields of NbN thin films fabricated at room temperature," Progress in Superconductivity and Cryogenics, vol. 17, no. 3, p. 9, 2015, doi: 10.9714/psac.2015.17.3.009.
[24] K. Choi, H. Choi, H. Na, and I. Sohn, "Effect of magnesium on the phase equilibria in magnesio-thermic reduction of Nb_2O_5," Materials Letters, vol. 183, p. 151, 2016, doi: 10.1016/j.matlet.2016.07.058.
[25] M. Jha, K. V. Ramanujachary, S. E. Lofland, G. Gupta, and A. K. Ganguli, "Novel borothermal process for the synthesis of nanocrystalline oxides and borides of niobium," Dalton Transactions, vol. 40, no. 31, p. 7879, Aug 21 2011, doi: 10.1039/c1dt10468c.
[26] A. Mozalev et al., "Formation–structure–properties of niobium-oxide nanocolumn arrays via self-organized anodization of sputter-deposited aluminum-on-niobium layers," Journal of Materials Chemistry C, vol. 2, no. 24, p. 4847, 2014, doi: 10.1039/c4tc00349g.
[27] T. Hryniewicz, K. Rokosz, and H. R. Z. Sandim, "SEM/EDX and XPS studies of niobium after electropolishing," Applied Surface Science, vol. 263, p. 357, 2012, doi: 10.1016/j.apsusc.2012.09.060.
[28] K. Zhussupbekov et al., "Oxidation of Nb(110): atomic structure of the NbO layer and its influence on further oxidation," Scientific Reports, vol. 10, no. 1, p. 3794, Mar 2 2020, doi: 10.1038/s41598-020-60508-2.
[29] T. Imamura and S. Hasuo, "Fabrication of high quality Nb/AlO_x-Al/Nb Josephson Junctions: Ⅱ-deposition of thin Al layers on Nb films," IEEE Transactions on Applied Superconductivity, vol. 2, no. 2, p. 84, 1992.
[30] X. Q. Jia et al., "High Performance Ultra-Thin Niobium Films for Superconducting Hot-Electron Devices," IEEE Transactions on Applied Superconductivity, vol. 23, no. 3, pp. 2300704-2300704, 2013, doi: 10.1109/tasc.2012.2235508.
[31] J. Yu et al., "Hydrothermally formed functional niobium oxide doped tungsten nanorods," Nanotechnology, vol. 24, no. 49, p. 495501, Dec 13 2013, doi: 10.1088/0957-4484/24/49/495501.
[32] C. C. Koch, J. O. Scarbrough, and D. M. Kroeger, "Effects of interstitial oxygen on the superconductivity of niobium," Physical Review B, vol. 9, no. 3, pp. 888-897, 1974, doi: 10.1103/PhysRevB.9.888.
[33] N. M. Jisrawi et al., "Reversible depression in the Tc of thin Nb films due to enhanced hydrogen adsorption," Physical Review B, vol. 58, no. 10, p. 6585, 1998.